IMECE2021-73376

OLIGODENDROCYTE TETHERING EFFECT ON HYPERELASTIC 3D RESPONSE OF INJURED AXONS IN BRAIN WHITE MATTER

Mohit Agarwal¹, Parameshwaran Pasupathy¹, Robert De Simone², and Assimina A. Pelegri^{1,*}

¹Rutgers, The State University of New Jersey Piscataway, NJ, USA

²Marotta Controls, Inc, 78 Boonton Avenue Montville, NJ, USA

ABSTRACT

Numerical simulations using non-linear hyper-elastic material models to describe interactions between brain white matter (axons and extra cellular matrix (ECM)) have enabled high-fidelity characterization of stress-strain response. In this paper, a novel finite element model (FEM) has been developed to study mechanical response of axons embedded in ECM when subjected to tensile loads under purely non-affine kinematic boundary conditions. FEM leveraging Ogden hyper-elastic material model is deployed to understand impact of parametrically varying oligodendrocyte-axon tethering and analyze influence of aging material characteristics on stress propagation. In proposed FEM, oligodendrocyte connections to axons are represented via spring-dashpot model, such tethering technique facilitates contact definition at various locations, parameterize connection points and vary stiffness of connection hubs. Two FE submodels are discussed: 1) multiple oligodendrocytes arbitrarily tethered to the nearest axons, and 2) single oligodendrocyte tethered to all axons at various locations. Root mean square deviation (RMSD) were computed between stress-strain plots to depict trends in mechanical response. Axonal stiffness was found to rise with increasing tethering, indicating role of oligodendrocytes in stress redistribution. Finally, stress state results for aging axon material, with varying stiffnesses and number of connections in FEM ensemble have also been discussed to demonstrate gradual softening of tissues.

Keywords: micromechanics, fatigue modeling, FEM, oligodendrocyte, TBI, axonal injury, CNS white matter, multiscale simulation, hyper-elastic materials, Abaqus

NOMENCLATURE

α	alpha
μ	shear moduli (hyper-elastic: Ogden model)
λ	principal stretches
σ	principal stress
G	complex shear modulus (viscoelastic model)
τ	shear stress
K	spring-dashpot stiffness

1. INTRODUCTION

Traumatic brain injury (TBI) can be defined as an acquired insult to the brain from an external mechanical force that could result in temporary or permanent impairment [1, 2]. TBI has been reported as leading cause of death and disability among children and young adults in the United States. It is estimated that 1.5 million Americans sustain a TBI annually [3], while at least 10 million serious enough TBI cases occur annually [4]. Often TBI results in a highly severe condition, because of excessive mechanical loading that might occur during vehicle accidents, sports injuries, violence, or injuries related to everyday activities. Moderate to severe TBIs can have long lasting or permanent effects such as cerebrovascular damage, neuronal deformation, hypoxia, cerebral edema, and increased intracranial pressure [5].

Brainstem and corpus callosum have been identified as most vulnerable to TBI. They are often subjected to high strains and susceptible to severe axonal damage [6]. Brain tissues show significant variations in overall material stiffness and critical regions have anisotropic material properties, which ultimately contribute to larger local deformations on the vulnerable sites. This is where finite element methods (FEM) steps in as a

^{*} Contact author: pelegri@rutgers.edu

prospective tool to model, characterize stress-strain response of the brain tissue and predict response to traumatic loading. Ever increasing computational capabilities have enabled in generating high fidelity models of microstructure of the brain. FEM for computational analysis of TBI date back to early 1970s (2D – FE models), while 3D FEM models burst onto the scene during 1990s [7]. Till date, a universal material model characterizing brain tissues have not been categorically identified, thus underlying the huge scope of improvement in the field of FEM based TBI modeling. Over the past decade, a wide spectrum of axonal material models has emerged ranging from linear elastic, viscoelastic to sophisticated hyper-elastic material models to define properties for brain soft matter. Moreover, hybrid techniques such as inverse finite element analysis to predict axonal material properties have also been proposed to identify material parameters to closest approximations [8-10]. TBI researchers have devoted significant effort in identifying optimal FE model geometry [11] and interfacing parameters between the axons and ECM to mimic actual stress transfer when subjected to traumatic loads [12]. Some of the early work in the field assumed affine boundary conditions to model the axons and ECMs whereby the axons are entirely tied down to the ECM. This however is a simplistic approximation since the axons and glia manifests a transitional behavior as a function of stretch/strain and along axonal tortuosity [2, 10].

Physiological aging of the brain results in gradual and progressive degeneration of its material properties. This degradation is experienced on all length scales, from the microstructural scales consisting of molecules and cells to the macroscopic tissue length levels. It has been reported that the loss of neurons due to age is around 10% [13]. Although the death of neurons is restricted due to normal aging, the ability of the cells to repair and regenerate tissues declines with time. Physiological degeneration of the brain cells, specifically, degradation of the neurons, surrounding matrix and the oligodendrocytes can be characterized by the change in the viscoelastic/hyper-elastic material models used to describe the brain tissue. Developing computational models of the brain which capture the effect of aging is crucial in gaining insight into age related brain atrophy. These models also enable researchers to compare the impact of brain injuries on healthy brains such as due to TBI with that of an aged brain. It has been reported that TBI can accelerate the aging process. The measured "brain age" of TBI brains have been estimated to be 4.66 years older than a normal healthy brain [14].

Central Nervous System (CNS) of the brain is composed of white and gray matter. White matter consists of myelin coated axons and oligodendrocytes. Axons are long slender projections of neuron which relays information to other neurons, muscles, and glands. Oligodendrocytes are glial cells which provide support and insulation to axons via sheath of myelin, which improves axonal stiffness. Influence of oligodendrocyte tethering on the mechanical response of the axons and ECM still requires elaborate investigation. In this study, a previously

published proof-of-concept FEM [2] has been investigated to understand effect of oligodendrocyte tethering on lowering stiffness response under non-affine boundary conditions in aging axons.

2. MATERIALS AND METHODS

2.1. Micromechanical Finite Element Model

The microscale FEMs are developed with the aid of Abaqus 2020 and Python scripting. The representative elemental volume (REV) for modeling axons tethered to glia in CNS white matter is based on the FE models developed by Pan et al. [2, 8]. Axons of varying undulation and radii are embedded in a 3D rectangular ECM with dimensions: $x=0.9~\mu m,~y=8~\mu m,~z=5.747~\mu m$. Undulation varies from axon to axon based on the work by Bain et al. [15], with average undulation varying from 1.00 to 1.10. The diameter of the axons vary from minimum of 0.4 μm to a maximum of 0.62 μm with an average axonal diameter of 0.45 μm . Following the same setup as used in previous work (see [2] for more details on FEM setup), non-affine boundary conditions between the axons and ECM are established using a "surface to surface" contact definition (see **Figure 1**) [16].

Oligodendrocytes produce *myelin* which wraps around the axons, insulate, and facilitate tethering amongst adjacent axons. Oligodendrocytes' bonding mechanisms and higher stiffness of myelinated axons are described in [2]. Glial cells provide mechanical support to embedded axons and dictate the response of the axons to tensile loading [15, 17, 18].

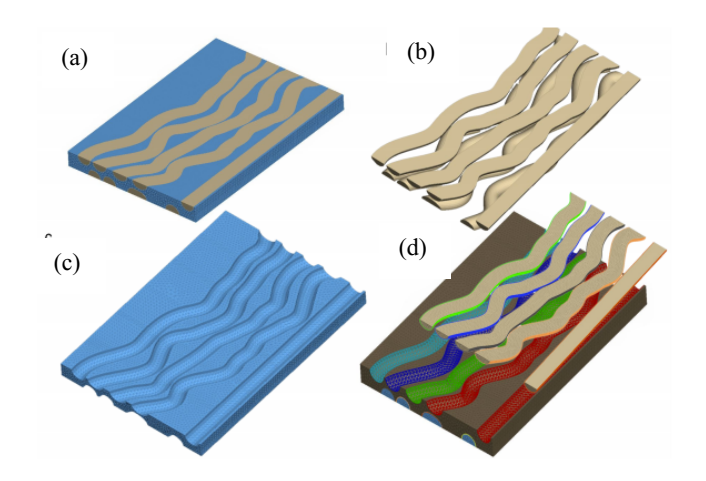


FIGURE 1: (a) FE Model of the ECM and axon assembly (b) FE model depicting the undulation of axons (c) FE model of ECM (d) Contact surfaces defining surface to surface contact between axons and ECM [2].

While myelination influence on axonal stiffness is well recorded, impact of varying tethering from oligodendrocytes on mechanical response of axons is still at its fledgling stage. Moreover, impact of aging CNS material properties on tethering model is an unchartered territory open to further exploration.

In the current study, our model analyzes oligodendrocyte tethering by simulating an ensemble of connection scenarios for two submodels (see **Figures 2a** and **2c**) outlined in later sections. Hyper-elastic material model parameters were improvised to incorporate aging/decaying of brain matter leveraging previously reported experimental MRI and MRE data [19, 20]. In total, four (4) sets of simulations are performed for normal and aging brain respectively, and trends in variation of mechanical response are analyzed. The same spring-dashpot approximation is used to model the arms of the oligodendrocyte that tether to the axons and distributed coupling constraints used for modeling the nucleus [2].

In the current model, oligodendrocytes are depicted as a distributed coupling of radius, $0.025~\mu m$ embedded inside the ECM. The reference node of the distributed coupling is located at the center of the sphere. The nodes of the ECM along the surface of the sphere act as coupling nodes (coupling constraints and contact definition used in FEM model can be found in [2]). A linear spring-dashpot connects different points along the length of the axon to the center of the oligodendrocyte sphere as shown in **Figure 2(b)**.

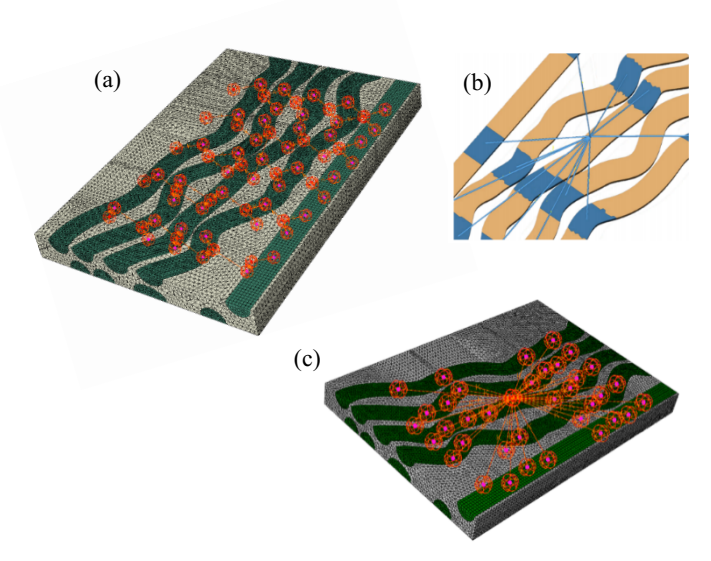


FIGURE 2: (a) Submodel-1: Oligodendrocytes arbitrarily tethered to axons, (b) a schematic representation of an oligodendrocyte tethering to axons at different locations via a sheath of myelin, (c) submodel-2: single oligodendrocyte tethering to surrounding axons.

2.2. Hyper-elastic Material Model

Nonlinear hyper-elastic models are commonly used for simulation of soft biological tissues [7, 8, 10, 21]. Some of the pioneering work in the field include Ogden hyper-elastic material model from Pan et al.[8-10] who simulated kinematics of CNS white matter, Karami et al. [11] who introduced embedded element approach and Mihai et al. [22] utilized experimental results to formulate hyper-elastic material models. While several hyper-elastic material models have been studied

in the recent past such as: Mooney-Rivlin [7], neo-Hookean, Demiray, Gent, and modified Ogden models [23], this paper, Ogden hyper-elastic material model is used to simulate the ECM and the axons [2]. The non-linearity of the Ogden model allows neural tissue to be characterized more accurately for large deformation and strains along with rate dependent behavior. The Ogden hyper-elastic model is based on the three principal stretches λ_1 , λ_2 , λ_3 and 2N material constants. The strain energy density function, W, for the Ogden material model (**Equation 1**) in Abaqus is formulated as [2, 16]:

$$W = \sum_{1}^{N} \frac{2\mu_{i}}{\alpha_{i}^{2}} \left(\lambda_{1}^{-\alpha_{i}} + \lambda_{2}^{-\alpha_{i}} + \lambda_{3}^{-\alpha_{i}} - 3 \right) + \sum_{1}^{N} \frac{1}{D_{i}} (J_{el} - 1)^{2i}$$
 (1)

where $\overline{\lambda_i} = J_{el}^{-\frac{1}{3}} \lambda_i$ and $\overline{\lambda_1 \lambda_2 \lambda_3} = 1$. μ_i represents shear moduli, while α_i and D_i are material parameters. The first and the second terms represent the deviatoric and hydrostatic components of the strain energy function. The parameter $D_i = \frac{2}{K_0}$, allows for the inclusion of compressibility where K_0 is the initial bulk modulus. An incompressible, single parameter Ogden hyper-elastic material is considered in this study. Therefore, N=1. Incompressibility implies that $J_{el}=1$ and is specified in Abaqus by setting $D_1=0$. As a result, Abaqus eliminates the hydrostatic component of the strain energy density equation, and the expression reduces to the following

$$W = \sum_{1}^{N} \frac{2\mu_{i}}{\alpha_{i}^{2}} \left(\lambda_{1}^{-\alpha_{i}} + \lambda_{2}^{-\alpha_{i}} + \lambda_{3}^{-\alpha_{i}} - 3 \right)$$
 (2)

Since the current model is based on uniaxial tension evaluation, the corresponding principal stress is expressed as:

$$\sigma_{uniaxial} = \frac{2\mu}{\alpha} \left[\lambda^{\alpha} - \left(\frac{1}{\sqrt{\lambda}} \right)^{\alpha} \right]$$
 (3)

Undulation prevents axons from experiencing full tension until the axon is straightened and the tortuosity becomes 1. In this study, the values for shear modulus for the axons and ECM are obtained from research by Wu et al. [24] while α is derived from the model developed by Meaney [21]. The shear modulus of the ECM is assigned relative to the shear modulus of the axon, considering axons are three times stiffer than ECM as reported by Arborgast and Margulies [6].

Table 1: Material properties of FE model

Component	μ MPa	<i>D</i> 1/ MPa	α	Element Type
Axon	2.15E-03	0	6.19	C3D8H C3D4H
ECM	8.5 E-04	0	6.19	C3D4H

Same approach as in [2], has been deployed to model incompressibility for the hyper-elastic material. Refer to **Table 1** for summary of material properties and element definition used in the FE model. In latter sections, change in parameters with respect to aging will be defined.

2.3. Hyper-elastic aging model

The tissues in the human brain become increasingly disorganized due to aging [19], primarily due to increasing loss of neurons and oligodendrocytes. These aging and atrophy effects on the non-linear hyper-elastic material properties in the brain matter significantly affect its mechanical response. To the knowledge of the authors, no published data is available which can be translated to a hyper-elastic material model to simulate mechanical response of an aging axon. Some research papers on experimental imaging of aging brain consider it to show predominantly viscoelastic behavior [19, 20, 25]. Experimental results from these sources have been used in adjusting the proposed hyper-elastic FE model to account for aging axon material properties.

In this study, only the shear moduli ' μ ' is assumed to be varying for characterizing an aging brain. In a 2009 study, Sack et al. reported that "healthy adult brain undergoes steady parenchymal 'liquefaction' characterized by a continuous decline in μ of 0.8% per year" [20]. Note: In their model, μ does not denote shear moduli, but a quantity like shear moduli, which describes the solid-fluid behavior of the tissues. For a typical viscoelastic material model, for small harmonically varying shear strain γ , is defined by $\gamma(t) = \gamma_0 \exp(i\omega t)$. The solution for shear stress $\tau(t)$ has the form (see **Equation 4**) and shear modulus is in the form of global complex modulus function denoted by $G(\omega)$ which comprises of real part - G'(storage)modulus) and G''(loss modulus) respectively, as represented in **Equation 5**[16]. As stated, since $G(\omega)$ is a complex quantity, the loss component cannot be disregarded and at the same time overall shear moduli $G(\omega)$ cannot be translated as $|G(\omega)|$ to represent μ in the hyper-elastic model.

$$\tau(t) = (G'(\omega) + iG''(\omega))\gamma_0 \exp(i\omega t)$$
 (4)

$$G(\omega) = G'(\omega) + iG''(\omega) \tag{5}$$

For small strains (< 5%), it is conjectured that stress-strain plot for hyper-elastic material model would closely resemble that of viscoelastic model. To test this hypothesis, proposed hyper-elastic micromechanical model is solved for steady-state dynamic (SSD) case and compared against viscoelastic model's stress-strain response at a fixed frequency (50 Hz). It is observed that both models overlap comprehensively (RMSD [2] value: 0.0000561), see **Figure 3**. Thus, decay, presented here as decrease in shear moduli (μ) for hyper-elastic model (**Equation 1**), is assumed to decline by 0.8% per annum to model stress-strain response for aging axons. Hence, shear moduli - $\mu(t)$ is

represented as function of age (time - t in years) and represented as per equation 6, where t_0 is age at t = 0 (initial condition).

$$\mu(t) = \mu(t_0)[1 - 0.008 * (t - t_0)] \tag{6}$$

While μ shows time-dependence decay, other parameters (α and D_i) [19, 20] in the model are assumed to remain constant with age. Time dependent decay in ' μ ' could be a higher order function. *Linear regression* fitting technique applied here is an attempt to describe a simple canonical form for the current study.

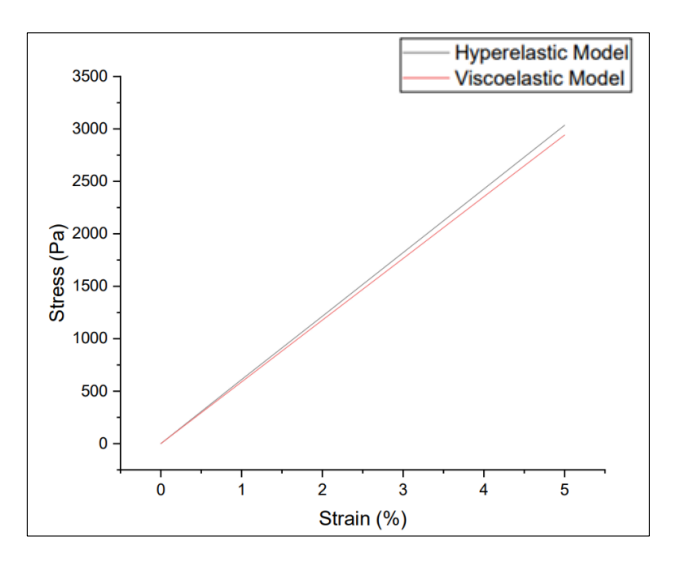


FIGURE 3: Overlapping hyper-elastic model (steady-state dynamic -SSD analysis at 50Hz) on the viscoelastic model (at 50Hz) to validate the proposed aging material characterization hypothesis.

2.4. Finite Element Submodels

In the current study, the two submodels presented in previous work [2] are further improved to study the effect of oligodendrocyte tethering on mechanical response of axons. For the first submodel (multi-oligodendrocyte case), a plane between the axon layers is created with 25 grid points equally spaced (see [2] for FEM geometrical configuration details). In the second (single-oligodendrocyte submodel case), oligodendrocyte ties to all the axons embedded at different sites. The sole oligodendrocyte is positioned at the center of the ECM. In this paper, connections between axons and oligodendrocyte are further parameterized to complete the ensemble and gain perspective on mechanical response for each connection configuration (see Figure 4). As outlined before, springdashpot elements simulate the tethering arms of the oligodendrocyte in proposed FEM [2]. Upon literature review, no published literature sources were found which could characterize oligodendrocyte stiffness. Hence, stress-strain response of the axons were obtained by parametric variation of spring-dashpot connection ('K'). The material properties of myelin served as the upper limit during parameterization of oligodendrocytes stiffness.

FE model Boundary Conditions: Symmetric boundary conditions are employed at the top and bottom faces in *x*-coordinate direction and side faces in *y*-coordinate direction. Constraints are applied in the *z*-direction using fixed boundary conditions (B.C.) on one face and a stretch is applied to the opposite face using a non-zero displacement boundary conditions An implicit time integration solver technique is used in Abaqus for computation. Contact stabilization prevents rigid body modes before contact is established between interacting surfaces of the axons and ECM [2].

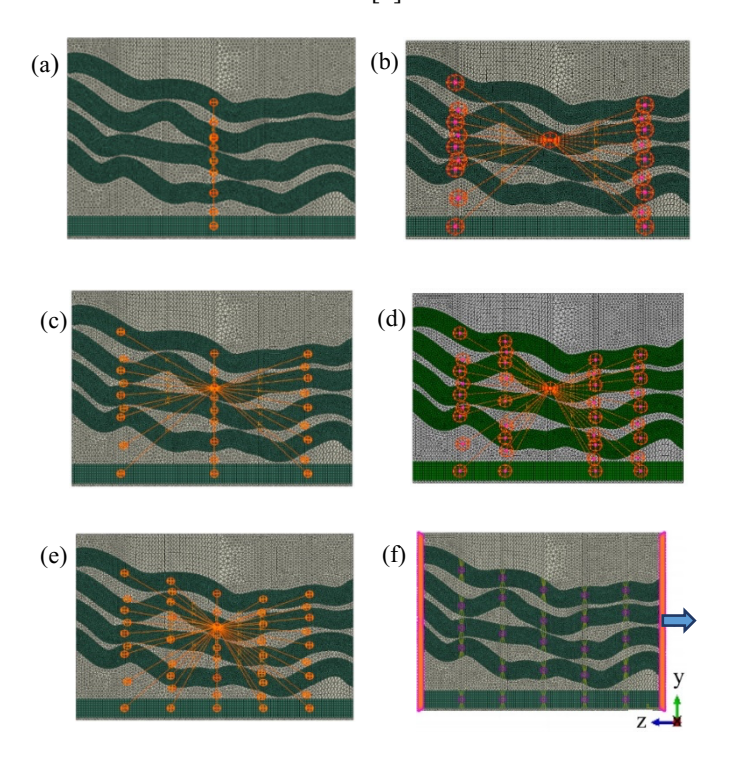


FIGURE 4: (a-e) Parameterization of number of connections between oligodendrocyte and each axon in submodel-2 showing 1, 2, 3, 4 and 5 connections per axon, (f) boundary conditions for the FE model with the left end fixed and a stretch applied on the right.

3. RESULTS AND DISCUSSION

For the present analysis, the developed micromechanical FE model is subjected to uniaxial stretch in the z-direction. As a representative case, FEM contour plots results with aging axon and ECM material combination for submodel-2 have been presented. The shear moduli for axon and ECM were defined for an individual of age 55 years (using **Equation 6** and **Table 2**). Specifically, 3-nodes per axon oligodendrocyte connection is selected as the sample case for analysis. For the chosen model, it is observed for 20% stretch case in z-direction that similar stress

contour plots were obtained (as in [2]) and tortuosity again prevents full extensions in axons (see **Figure 5**) [26].

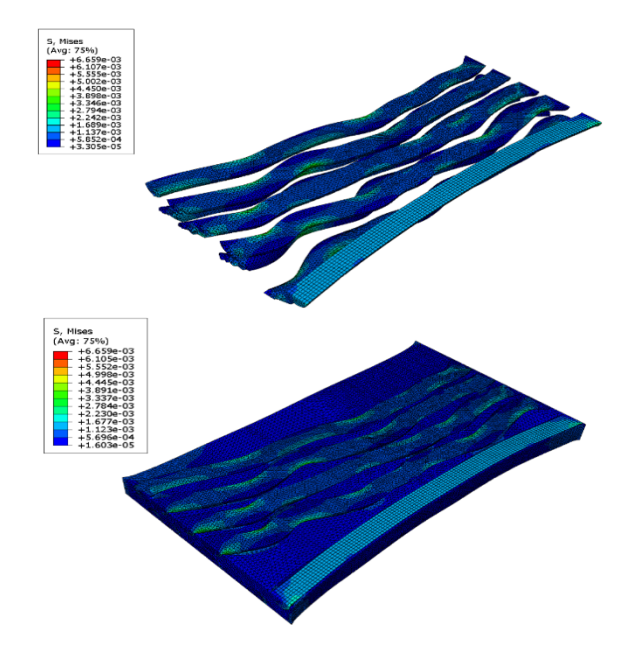


FIGURE 5: Von Mises stress contour for the axons and the ECM at 20% applied stretch for 3-nodes per axon (submodel-2 – single oligodendrocyte) aging axon material property bearing FE micro-mechanical model. Undulation of axons resulting in high stress in the concave regions also observed in case of aging axons.

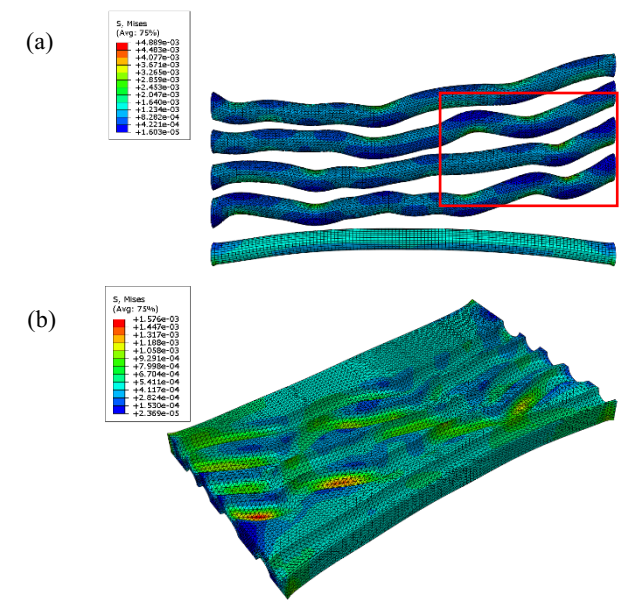


FIGURE 6: (a) Bending stresses undergoing full reversal (see rectangular marked region) from tension to compression for FE-micromechanical with aging axon & ECM material properties (b) von-Mises stress contour plot exclusive for ECM.

For the aging case, straight axon (**Figure 5**) is in full tension while the undulated axons experience bending stresses along its tortuous path (see [2] for effect of bending stress). Presence of bending stresses increases the risk of fatigue failure. Due to gradual softening of tissues, von-Misses stress values are observed to be approximately 30% lower in aging axon-ECM material FE models (see **Figure 6**) when compared to previous results [2]. Even though current results does not account for any fatigue or cumulative damages on axonal injuries, numerical results obtained using aging axon-ECM FE material model may serve as reference for any future study related to full-scale fatigue analysis of aging brain.

As discussed in Section 2.1, submodel-1 contains total 25 oligodendrocyte spheres tethering to the nearest axons (total 69 connections). On the other hand, submodel-2 contains a single oligodendrocyte at the FE model center tethered to all the axons (number of connections can be parametrically varied).

3.1. Submodel-1 analysis outcomes:

For the multi-oligodendrocyte (submodel-1) FE model, detailed inspection was done by computing stress-strain behavior for varying spring-dashpot stiffness. The spring-dashpot connection is parameterized for different stiffness values. K=10, 50, 75 and 100 N/m. To present the significance of these stiffness values (K) from a physiological context, K=10 N/m represents a tethering connection that is 300 times weaker than the ECM. From applied force point of view, this variation can be described as: to produce a net strain of, for example, 10% (i.e., $0.568 \mu m$), minimum load required will vary in the ratio 1:5:10 for 10K:50K:100K models (simply denoting 10 N/m as 10K and so forth). These stiffnesses are much lower than traditional macrocomponent level springs observed in everyday assemblies but from the context of brain matter strain energy variations they bring significant variations in the micromechanical FE model.

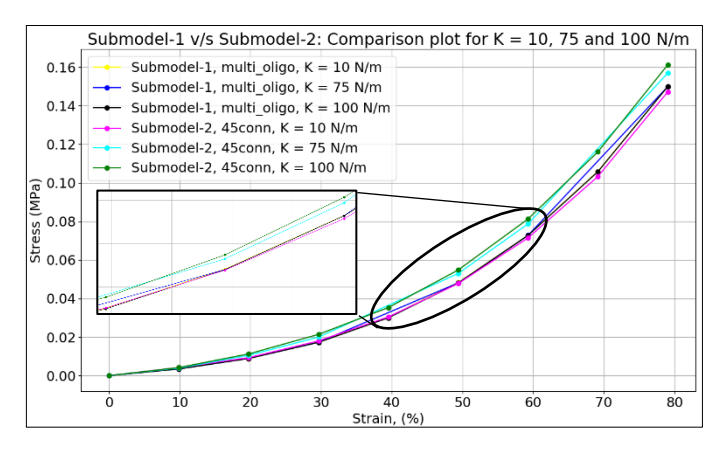


FIGURE 7: Stress (σ) versus stretch plot for both multioligodendrocyte (submodel-1) and single-oligodendrocyte (submodel -2) FEM plotted for varying spring-dashpot stiffness (K) parameters up to 80% strain. Submodel-1 showing indistinguishable change in mechanical response with varying K. Moreover, submodel-2 proved to be stiffer for higher K values.

Figure 7 depicts the combined plot for multioligodendrocyte micromechanical models (submodel-1) which were solved up to 4x (80%) strain/stretch limit. It was observed that mechanical response variations were indistinguishable even with varying oligodendrocyte arm stiffness (K). This is because in submodel-1, all connections between the oligodendrocytes and the axons are in xy-plane and perpendicular to z-direction. As the model deforms (stretches along z-axis), the springs do not experience any net deformation along z (which would have been the primary direction contributing to stiffening the axonal mechanical response). Thus, both end nodes of the springs move by the same amount in z-direction. The only response that the springs provide is in y-direction (i.e., opposing compression due to Poisson's effect along *y-axis*). As previously reported both sub models behave similarly[2] for very low spring stiffness values. This observation was based on limited data and as we have expanded the data pool, the current investigation reveals that for higher spring stiffnesses (K = 100 N/m), submodel-2 exhibits markedly stiffened response.

As shown in **Figure 7**, at K=10N/m, stress-strain response for sub-models 1, 2 are on top of each other. But, upon increasing the stiffness to K=75 N/m and 100 N/m submodel-2 showed an increasingly stiffened response (as expected). This also aligns with observations drawn in Section 3.3 (see **Figure 10**). Thus, the analysis surfaces an inherent limitation in submodel-1. In future, a more randomized modelling of springs in submodel-1 could resolve the observed deviations for higher K values. Meanwhile, RMSD values between 10K and 100K submodel-1 curves is found to be very minimal (0.00015). Comparative analysis between submodel-1 and submodel-2 revealed that RMSD for the two models with K=10 N/m is 0.00139, at K=75 N/m (RMSD: 0.0041) and for K=100 N/m RMSD between submodels -1,2 increased to 0.00710, Thus, supporting the discussed claims on expected submodel-1 behavior.

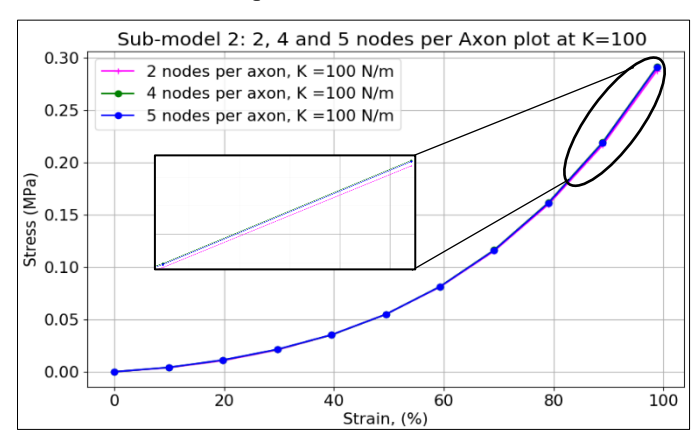


FIGURE 8: Impact of parameterization (change in number of connections between oligo and axons) evaluated by overlaying 36 connections (4-nodes per axon),18 connections (2-nodes per axon) and 45 connections (5-nodes per axon) submodel-2 results at spring-dashpot stiffness value $K=100~{\rm N/m}$ value and subsequent RMSD analysis done on the results to quantify relative increase in axonal stiffness.

3.2. Submodel-2 analysis outcomes:

The effect of parametric change in number of connections in submodel-2 is evaluated through a comparison plot of the stress-strain response (see figure 8), keeping set spring-dashpot stiffness value at K=100 N/m. Here, submodel-2 plot shown covers three scenarios: 2, 4 and 5 oligodendrocyte connections per axon. Current numerical analyses consolidate the previous inferences [2] by including the remaining cases (2-nodes and 4nodes per axon) to gain complete perspective on submodel -2's characteristic mechanical response. Varying number of connections do not have any significant effect on the mechanical response rather all stress-strain curves seem to collapse on one another. Only upon closer inspection, this modest increase in axonal stiffness becomes apparent. These trends correlate with the previous results [2]. From Figure 8, it can be ascertained that for FE submodel-2, increasing tethering contributes to greater stiffness of the axons.

The RMSD between the curves showed minor increment, i.e., root mean square deviation (RMSD) between the 18 connections (2-nodes per axon) and 36 connections (4-nodes per axon) curves is 0.00158, where RMSD is defined as $\sqrt{\sum \frac{(f(x_i)-g(x_i)^2}{N}}$ for curves f(x), g(x) and N being number of points x_i at which curves are compared. For brevity, denote the two curves as 2-4. Similar RMSD analysis for other curves revealed that differences in stress-strain response diminishes as higher connection configurations are compared (i.e., RMSD values between 4-5 is 0.00038 < 2-5 (RMSD: 0.00123) curves).

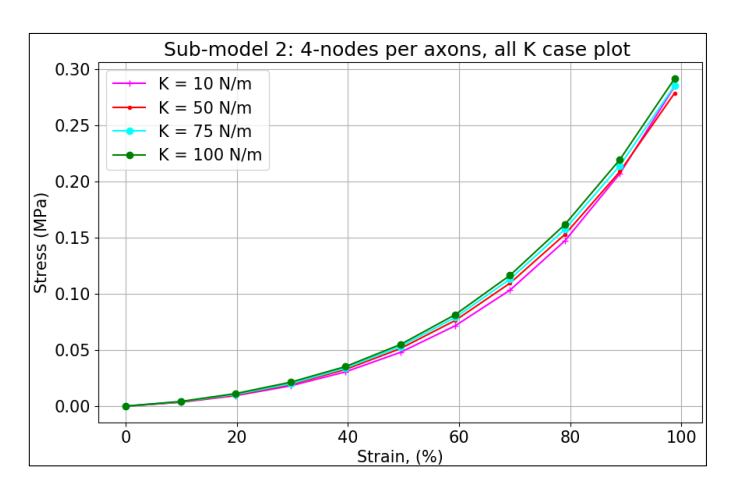


FIGURE 9: Stress-strain response for submodel-2 (single-oligodendrocyte) parameterizing the spring-dashpot stiffness (K) of the oligodendrocyte arms. Simulations performed for 4 oligodendrocyte connections per axon (36 connections) for K = 10, 50, 75 and 100 N/m, respectively. Trend in agreement with the stress-strain response observed for 5 oligodendrocyte connections per axon [2].

For submodel-2, results for mechanical response at varying stiffness values of oligodendrocyte arms were also examined.

For a given number of connections per axon (4 nodes per axon in this case), it was seen that by increasing "K", the stress-strain plot exhibited greater stiffness (refer **Figure 9**), when subjected to strains up to maximum of 100% applied stretch. Model becomes progressively stiffer for higher values of "K". RMSD between 10K and 50K (0.00368) < RMSD between 10K and 75K curves (0.0056) < RMSD between 10K and 100K (0.00837). Again, validating the argument that the oligodendrocytes do act as a supporting scaffold for the axons in addition to the stiffening provided by the myelin sheath [2]. The simulations were executed for 2-nodes and 4-nodes per axon tethering cases and same conclusions were drawn.

3.3. Submodel-1 versus submodel-2:

Both the micromechanical FE models generate very identical stress-strain response, although some contrasting results are observed in terms of relative stiffness in response to tensile loads. In the previous study, multi-oligodendrocyte models proved to be slightly stiffer than single-oligo model but simulating 4-node per axon (36 connections) FE model with K =100 N/m revealed that single-oligodendrocyte model (submodel-2) is stiffer than multi-oligodendrocyte model (see **Figure 10**). RMSD between the two curves being 0.00685. This reversal in trend could be due to the geometrical differences in the two model, for sufficiently stiffened model (such as 36 connections -4 nodes per axon model), the spring-dashpot network at K =100 N/m is tethered to oligodendrocyte at the center and each spring-dashpot connection is subjected to greater relative stretch when compared to the stretch experienced in submodel-1 (multioligodendrocyte case). Thus, indicating greater axonal stiffness for submodel-2 when evaluated for K = 100 N/m case.

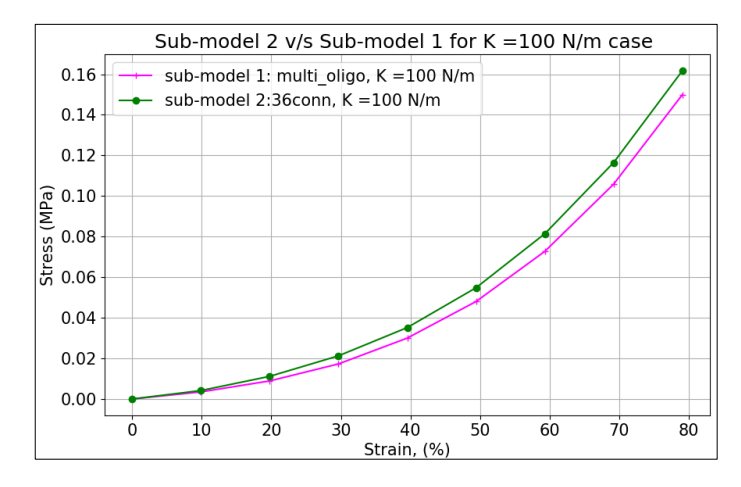


FIGURE 10: Submodel-1 (multi-oligo model with total 69 connections) versus submodel-2 (4-connections per axon, total 36 connections) plotted and submodel-2 found to yield greater axonal stiffening. The two models were compared with a constant value of spring-dashpot stiffness value K = 100 N/m. (RMSD value: 0.006846)

In the previous study[2], two submodels were compared at K = 10 N/m[2] while **Figure 10** plots stress-strain response at

K=100 N/m (more stiffened initial spring-dashpot geometrical set up). This marked variation in axonal stiffness between submodel-2 and submodel-1 at higher K values is counterintuitive. The reasons for it have already been pointed out in Sections 3.1 and 3.5 during the discussion of submodel-1 and its inherent geometrical limitations. Thus, no unequivocal inferences can be drawn on submodel stiffness comparisons, instead factors such as number of connections, geometrical setup of the FE submodel and spring-dashpot stiffness value overall influence resultant axonal stiffness. As part of future research, one possible exploration area could be to further investigate the relative change in stiffness on case-by-case basis by cautious change of key parameters and a revised submodel-1 having randomized spring-dashpot connections to draw statistically significant conclusions on relative submodel superiority.

In logical congruence with previous work (i.e., **Figures 8-9** in [2]) it can be acknowledged as an initial inference that for nearly the same number of total oligodendrocyte connections per axon, the stress response is almost identical in both submodels (especially for lower set spring-dashpot stiffness values). But latest set of results distinctly indicate that along with number of connections, set value of oligodendrocyte connection arm stiffness also influences the resultant mechanical response. Thus, exhaustive evaluation of the entire FEM ensemble reveals that single-oligodendrocyte models (submodel-2) could yield stiffer axon-ECM models for higher number of connections and higher *K* values (**Figure 10**). In terms of pure magnitude, the values could lie in the same range, but relative stiffness discrepancies become prominent on close inspection by RMSD analysis.

3.4. Aging/injured brain - hyper-elastic model analysis:

In this paper, the proposed FE models is also leveraged to evaluate mechanical response of brain matter for aging axon and ECM hyper-elastic material properties. Typical aging related degeneration of neurons and oligodendrocytes is inevitable and experimental data suggest that this decline in whole-brain elasticity is predominantly linear (0.8% per annum) [19, 20]. Some of the pioneering experimental research in the domain based on Magnetic Resonance Elastography (MRE) techniques have advocated brain/CNS (central nervous system) matter to be predominantly viscoelastic, but direct translation of viscoelastic properties into a hyper-elastic material model is not trivial.

Table 2: Parameter variation for aging FE Model

Age (years)	Axon Shear moduli μ_{axon} (MPa)	ECM shear moduli μ_{ECM} (MPa)
18	2.15E-03	8.50E-04
55	1.51E-03	5.98E-04

As discussed in Section 2.3, cautious transfer of material parameters is envisaged to tackle this FEM problem to predict

aging brain's response to traumatic load and plot stress-strain graphs for aging axons and ECMs. Refer to **Table 2** for shear moduli values for axons and ECM. In this analysis, a young healthy adult's (age 18 years) micromechanical model is compared against an elderly person's (age 55 years) model for the same boundary conditions.

As a representative case scenario for the sake of the analysis, 3-nodes per axon connection case from submodel-2 is selected for FE analysis. The static loading simulation (tensile load is applied in z-direction) and stress versus stretch response were recorded for both young and aged micromechanical FE model. It is observed that there is distinct loss in axonal stiffness over age (**Figure 11**), and RMSD value between the curve is 0.03672.

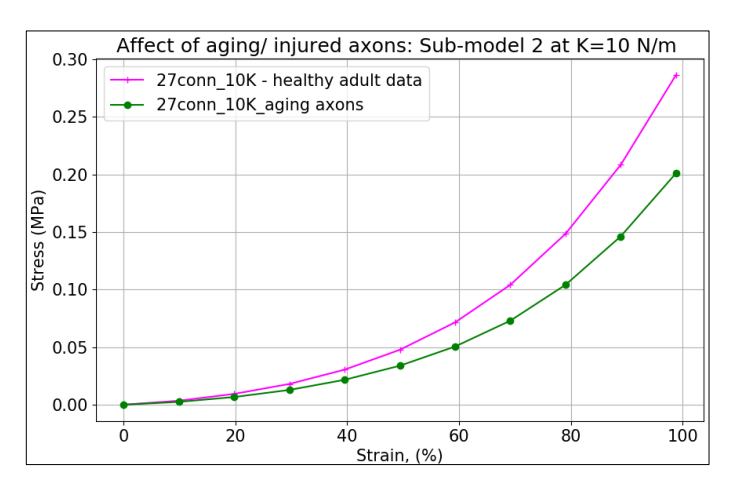


FIGURE 11: Submodel-2 (single oligodendrocyte case) for 3 connection per axons (27 total connections) configuration at K = 10 N/m was analyzed for both young (18 years old individual) and aged individual (55 years) by considering aging axonal material parameters. Distinct loss of stiffening due to aging noticed for aged material data plot, showing influence of aging on axonal stress-response.

Due to aging, there is a steady decline observed in the max stress generated due to the gradual softening of the axon and ECM tissues. This is reflected in the linear decay plot of max stress versus age graph (Figure 12). To obtain the stress versus age plot, from single oligo FE submodel (submodel-2) 3-nodes per axon case is chosen. A nominal strain is applied, 1x here (20%). Stress versus stretch is computed for gradually aging human being, i.e., FE simulation of the same loading case in 5 years interval, starting at age 18 till the age of 55 years. Total 9 data points are obtained (for varying ages: 18, 23, 28, 33, 38, 43, 48, 53 and 55 years). A linear decay in max. stress is observed. This linear decay observed is purely because the aging model is only incorporating change in ' μ ' over time (refer section 2.3). Since there is lack of any experimentally verified data depicting variation for material parameters such as ' α ' and 'K' as function of time/ age. Hence, as a first step in understanding aging brain characteristics only depreciation of ' μ ' has been considered in the proposed model. However, it does not imply that max. stress vs age will always follow a linear depreciation. Higher order decay characteristics could be incorporated if a verified time decay function for ' α ' and 'K' parameters in the hyper-elastic material model can be obtained from experimental data.

Research on characterization of aging brain white matter's mechanical response is still evolving. The current study is one such attempt towards synthesis of high-fidelity numerical models to predict impact of aging and atrophy. The solutions presented here are not exhaustive and merits further exploration. The current approach, however, is first of its kind that aims to cautiously fuse in parameters from two elasticity constitutive models and can serve as a foundation to further research in the area.

To reiterate, in this study the focus was limited to characterize the impact on axonal stiffening courtesy of oligodendrocyte tethering and not the oligodendrocyte itself [2]. Results corresponding to axonal stiffening correlated perfectly with trends observed in previous studies in the domain [2, 10]. In the current model, each defined connection between an oligodendrocyte and the axon creates such nodes of Ranvier. An increasing number of such connections imply a greater number of nodes being created and thus, a stiffer axon. These results apply for both young and aging axons.

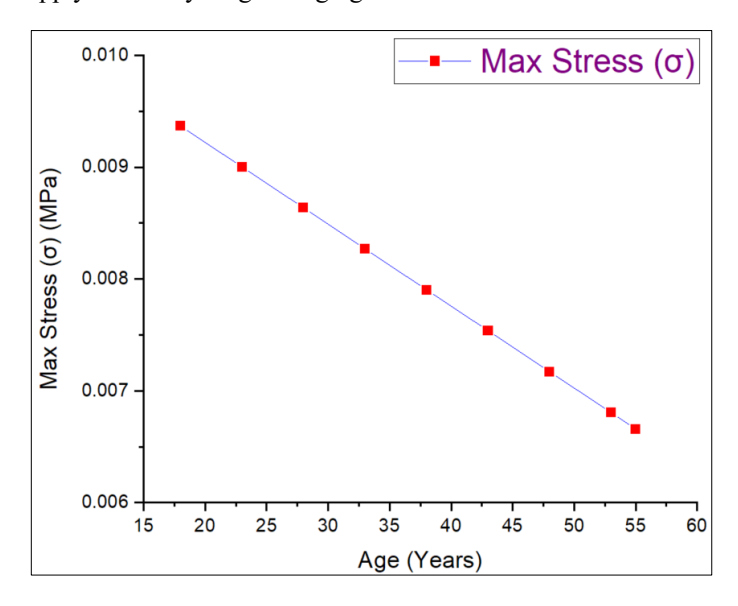


FIGURE 12: Decrease in maximum stress generated in the softened axon-ECM tissues depicted through max stress versus age plot. The proposed aging brain FE model only incorporates depreciation of '\(\mu\)' over time[20] in the hyper-elastic material constitutive equation to yield a linear depreciation in stress over age.

3.5. Model Limitations and Assumptions:

The proposed FE model has potential limitations. To begin with, the model approximated pure non-affine boundary conditions for entire stretch history, even though physiologically axons tend to exhibit more of transitional behavior. Thus, future

FE models incorporating transition mechanism could yield high fidelity results[2]. The current study approximates oligodendrocyte-axonal tethering by linear spring-dashpot connections. Geometrical limitations of submodel-1 have also been acknowledged in Sections 3.1 and 3.3 to explain indistinguishability in mechanical response variations with varying K values (Figure 7) and lower axonal stiffness observed in submodel-1 when compared against submodel-2 (Figure 7 and 10). Since, the geometrical setup of submodel-1 involves all connections between the oligodendrocytes and axons in xy-plane (perpendicular to z-direction), springs do not experience any net deformation along z-direction. Hence, submodels-1 and submodels-2 show similar behavior at lower spring stiffness values but upon increasing the K values, submodel-2 depicted an increasingly stiffened response. A revised submodel-1 is in the works to resolve such deviations by incorporating more randomized modelling of springs. Next, for the aging micromechanical FE models, atrophy affects are only accounted in axons and ECM but not in oligodendrocytes. For aging brain analysis, impact of degradation on α and K was not factored in. Thus, Figure 12 projected a linear depreciation in max stress but as elucidated in section 3.4, the aging model yielded linear decay because current model only incorporates change in u with respect to age (t) as backed by data from Sack and et al. [20]. As stated previously, non-linear decay characteristics could be incorporated in the study of aging brain matter's mechanical response if verified time decay functions for ' α ' and 'K' parameters in the hyper-elastic material model can be obtained from experimental data. In the current set of simulations, damage initiation and evolution were not discussed either.

4. CONCLUSIONS

In the current study, the proposed 3D simulation framework comprising of two FE submodels are presented. An ensemble of simulation scenarios for both submodels describing the tethering of oligodendrocytes to axons have been executed. These simulations were performed for both young and aged conditions of brain matter. For both young and aged axon material properties, numerical results indicate appearance of bending stresses along their tortuous path [2] with stress reversal. Irrespective of submodel chosen, resultant bending stress magnitude or pertinent cerebral damage is dependent on axon geometry, variation in brain mass, loading direction and current state of the shear moduli (impact of aging, injury, or atrophy).

Parametrization of oligodendrocyte connections for the ensemble of cases in both submodel types indicate that axons exhibit greater stiffness with increasing number of connections. However, not only increasing oligodendrocyte-axon tethering connections but also greater oligodendrocyte arm stiffness "K value" in tandem enable increment in axonal stiffness. As ascertained in the previous study, this trend could be attributed to creation of nodes of Ranvier, which aids in this increment [2]. Thus, oligodendrocyte connections are instrumental in improving stress-strain response to external loading. While from a physiological standpoint, it is firmly established that

oligodendrocytes support axons by covering them with sheath of myelin, but their tethering to axons too perhaps plays an important role in improving axonal stiffness.

While proposed FE model has room for further improvements, it serves adequately as proof-of-concept model to understand mechanical response of axons and ECMs. Moreover, the presented submodels can be customized to not only incorporate range of mechanical properties for axons and ECM, but also evaluate transitional behavioral mechanism (affine to non-affine boundary conditions) to yield high fidelity results [2]. Next, oligodendrocyte-axonal tethering could be replaced with non-linear spring-dashpot connection type. Current hyper-elastic model can be adjusted to incorporate impact of variations in ' α ' and study corresponding non-linearity introduced by it. As a future research objective in aging brain analysis, further exploration to parametrically determine influence of changing constitutive material model parameters on aging brain matter's mechanical response could be undertaken.

An extension on current set of results, with an exhaustive FE setup bearing non-linear connection types and material parameters could help answer pressing questions in relation to damage initiation and evolution for both healthy and aging brain. Such an elaborate FE model would facilitate depict repair and recovery mechanisms and abilities for both young and aged brain. Lastly, devising 3D FE model incorporating damage accumulation and fatigue behavior would provide a comprehensive understanding of structural response of young, aging, or injured axons to external loads.

ACKNOWLEDGEMENTS

Support was provided by NSF Grants CMMI-1436743, CMMI-1437113, CMMI-1762774, CMMI-1763005, an NSF graduate research fellowship award to N. M. Naughton, and the R.A. Pritzker endowed chair.

REFERENCES

- [1] Capizzi, A., Woo, J., and Verduzco-Gutierrez, M., 2020, "Traumatic Brain Injury: An Overview of Epidemiology, Pathophysiology, and Medical Management". *The Medical clinics of North America*, **104**(2),0025-7125, pp. 213-238
- [2] Pasupathy, P., De Simone, R., and Pelegri, A.A. 2020. "Numerical Simulation of Stress States in White Matter via a Continuum Model of 3D Axons Tethered to Glia". in ASME 2020 International Mechanical Engineering Congress and Exposition. Portland, OR, USA: ASME, Volume 5: Biomedical and Biotechnology, V005T05A038
- [3] Thurman, D.J., 1999, "Traumatic brain injury in the United States; a report to Congress".
- [4] Langlois, J.A., Rutland-Brown, W., and Wald, M.M., 2006, "The epidemiology and impact of traumatic brain injury: a

- brief overview". *The Journal of head trauma rehabilitation*, **21**(5),0885-9701, pp. 375-378
- [5] Ratajczak, M., Ptak, M., Chybowski, L., Gawdzińska, K., and Będziński, R., 2019, "Material and structural modeling aspects of brain tissue deformation under dynamic loads". *Materials*, 12(2), p. 271
- [6] Arbogast, K.B. and Margulies, S.S., 1998, "Material characterization of the brainstem from oscillatory shear tests". *Journal of Biomechanics*, 31(9),0021-9290, pp. 801-807
- [7] Brooks, T., Choi, J.E., Garnich, M., Hammer, N., Waddell, J.N., Duncan, W., and Jermy, M., 2018, "Finite element models and material data for analysis of infant head impacts". *Helivon*, 4(12),2405-8440, p. e01010
- [8] Pan, Y., Sullivan, D., Shreiber, D.I., and Pelegri, A.A., 2013, "Finite element modeling of CNS white matter kinematics: use of a 3D RVE to determine material properties". Frontiers in bioengineering biotechnology, 1,2296-4185, p. 19
- [9] Singh, S., Pelegri, A.A., and Shreiber, D.I., 2015, "Characterization of the three-dimensional kinematic behavior of axons in central nervous system white matter". *Biomechanics modeling in mechanobiology*, 14(6),1617-7940, pp. 1303-1315
- [10] Pan, Y., Shreiber, D.I., and Pelegri, A.A., 2011, "A transition model for finite element simulation of kinematics of central nervous system white matter". *IEEE transactions on biomedical engineering*, **58**(12),0018-9294, pp. 3443-3446
- [11] Karami, G., Grundman, N., Abolfathi, N., Naik, A., and Ziejewski, M., 2009, "A micromechanical hyperelastic modeling of brain white matter under large deformation". *Journal of the mechanical behavior of biomedical materials*, 2(3),1751-6161, pp. 243-254
- [12] Yousefsani, S.A., Shamloo, A., and Farahmand, F., 2018, "Micromechanics of brain white matter tissue: a fiber-reinforced hyperelastic model using embedded element technique". *Journal of the mechanical behavior of biomedical materials*, **80**,1751-6161, pp. 194-202
- [13] Morrison, J.H. and Hof, P.R., 1997, "Life and death of neurons in the aging brain". Science, 278(5337),0036-8075, pp. 412-419
- [14] Cole, J.H., Leech, R., and Sharp, D.J., 2015, "Prediction of brain age suggests accelerated atrophy after traumatic brain injury". *Annals of neurology*, 77(4),0364-5134, pp. 571-581
- [15] Bain, A.C. and Meaney, D.F., 2000, "Tissue-level thresholds for axonal damage in an experimental model of central nervous system white matter injury". *Journal of biomechanical engineering*, **122**(6),0148-0731, pp. 615-622
- [16] Abaqus, U.m.M., Standard, 2005, "Hibbitt, Karlsson, and Sorensen", 8,
- [17] Hao, H. and Shreiber, D., 2007, "Axon kinematics change during growth and development". *Journal of biomechanical engineering*, **129**(4),0148-0731, pp. 511-522
- [18] Shreiber, D.I., Hao, H., and Elias, R.A., 2009, "Probing the influence of myelin and glia on the tensile properties of the

- spinal cord". *Biomechanics modeling in mechanobiology*, **8**(4),1617-7940, pp. 311-321
- [19] Sack, I., Streitberger, K.-J., Krefting, D., Paul, F., and Braun, J., 2011, "The influence of physiological aging and atrophy on brain viscoelastic properties in humans". *PloS one*, 6(9),1932-6203, p. e23451
- [20] Sack, I., Beierbach, B., Wuerfel, J., Klatt, D., Hamhaber, U., Papazoglou, S., Martus, P., and Braun, J., 2009, "The impact of aging and gender on brain viscoelasticity". *Neuroimage*, **46**(3),1053-8119, pp. 652-657
- [21] Meaney, D.F., 2003, "Relationship between structural modeling and hyperelastic material behavior: application to CNS white matter". Biomechanics modeling in mechanobiology, 1(4), pp. 279-293
- [22] Mihai, L.A., Budday, S., Holzapfel, G.A., Kuhl, E., and Goriely, A., 2017, "A family of hyperelastic models for human brain tissue". *Journal of the Mechanics and Physics* of Solids, 106,0022-5096, pp. 60-79
- [23] Budday, S., Ovaert, T.C., Holzapfel, G.A., Steinmann, P., and Kuhl, E., 2019, "Fifty shades of brain: a review on the mechanical testing and modeling of brain tissue". Archives of Computational Methods in Engineering, 27,1886-1784, pp. 1187–1230
- [24] Wu, X., Georgiadis, J.G., and Pelegri, A.A. 2019. "Brain White Matter Model of Orthotropic Viscoelastic Properties in Frequency Domain". in ASME International Mechanical Engineering Congress and Exposition. American Society of Mechanical Engineers, 59407, p. V003T004A024
- [25] Sullivan, D.J., Wu, X., Gallo, N.R., Naughton, N.M., Georgiadis, J.G., and Pelegri, A.A., 2021, "Sensitivity analysis of effective transverse shear viscoelastic and diffusional properties of myelinated white matter". *Physics* in Medicine Biology, 66(3),0031-9155, p. 035027
- [26] Bain, A.C., Shreiber, D.I., and Meaney, D.F., 2003, "Modeling of microstructural kinematics during simple elongation of central nervous system tissue". *Journal of biomechanical engineering*, **125**(6),0148-0731, pp. 798-804